Thermal Performance of a High-flux Solar Concentrating System

M. Mouzouris[a], L.W. Roberts[b] and M.J. Brooks[b]

Received 20 April 2011 and accepted 5 December 2011

A point-focus concentrator is described for collecting and transporting solar energy at flux levels exceeding 100 W/cm^2. The Fibre Optic Concentrating Utilisation System (FOCUS) comprises a 600 mm diameter ring array concentrator injecting solar rays into an optical waveguide for transmission to a remote target. The ring array incorporates a nested set of paraboloidal elements, each with appropriate geometry to reflect sunlight to a common focal point. The use of composite materials in manufacturing the concentrator enables a low-cost solution with good rigidity, giving measured surface slope errors of between 2.90 mrad and 5.39 mrad rms. Optical ray tracing is used to generate a system performance model which is compared with experimental data obtained using energy balance methods and a flat plate calorimeter. Temperatures exceeding 1200 K and a concentration ratio approaching 1800 suns are achieved, demonstrating the collector's usefulness in high-flux research applications. The study shows that useful solar flux can be delivered by low-cost concentrators fabricated from composite materials. Among other applications, the system is intended for use in lunar in-situ resource utilisation research, where lunar soil simulants are melted for oxygen production, surface stabilisation and related activities.

Additional Keywords: Ring array concentrator, high-flux solar calorimetry, in-situ resource utilisation

Nomenclature

Roman

C	concentration ratio
F	flux [W/cm^2]
$\dot{m}$	mass flow rate [kg/s]
n	refractive index
P	power [W]
q	solar power [W]
T	temperature [°C]

Greek

α	absorptivity
η	efficiency
τ	transmission

Subscripts

abs	absorbed
act	actual
foc	focus
inj	injection
in	inlet
l	losses
out	outlet
s	copper plate surface

Abbreviations

CMM	co-ordinate measuring machine
CPV	concentrating photovoltaic
DNI	direct normal irradiance
FOCUS	fibre optic concentrating utilisation system
ISRU	in-situ resource utilisation
OW	optical waveguide
RAC	ring array concentrator
RMSE	root mean square error

a MScEng student
a,b School of Mechanical Engineering
University of KwaZulu-Natal, Durban, 4041.
E-mail: brooks@ukzn.ac.za

1. Introduction

Solar collectors are used to capture solar radiation and transform the energy into heat for diverse applications such as electricity production and generation of hydrogen[1]. They are categorised either as non-concentrating, for example the flat plate variety used in solar water heating applications, or concentrating, such as those collectors employed for high-heat-flux applications[2]. Concentrating collectors are further classified into line focus or point focus systems[3]. Point focus technologies include parabolic dishes and central receivers that can achieve temperatures in excess of 1500 °C and are mainly based on the parabolic reflector dish, as the primary concentrator[2]. A novel point focus collector introduced by Vasylyev and Vasylyev[4] is the ring array concentrator, which provides high concentration with single stage reflection and is suitable for smaller-scale research initiatives. Advantages over the commonly used dish include rearward focusing and the potential to outperform the dish geometry at shorter focal lengths[5]. The ring array configuration is formed by a set of concentrically nested paraboloidal elements that operate similarly to a Fresnel lens to converge solar rays to a common point (figure 1). Unlike a Fresnel lens, the sunlight

is reflected, not refracted, therefore optical losses are reduced.

To date, a number of designs have demonstrated the use of point focus technology to concentrate solar energy into fibre optic cables. Feuermann *et al.*[6] performed experiments using a 200 mm diameter parabolic dish coupled to an optical

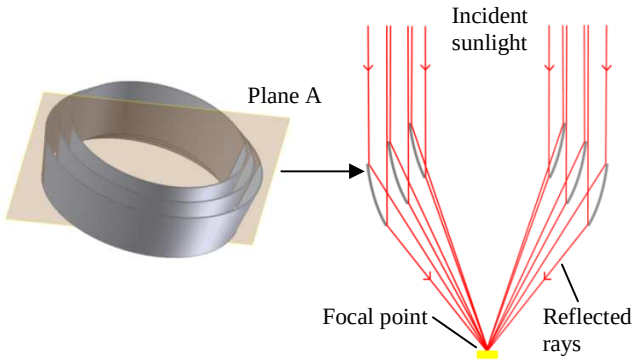

Figure 1: Typical paraboloidal elements of a ring array concentrator – three element profiles single stage reflection to a common focal point.

fibre 1 mm in diameter that achieved power densities of 1000 W/cm^2 for solar surgery. Nakamura and Senior[7] constructed an optical waveguide (OW) solar thermal system for lunar materials processing. Their system consists of seven 27-inch parabolic mirrors concentrating solar energy into optical fibres to deliver a flux of 137 W/cm^2 for the production of oxygen from lunar regolith. The present work differs from existing efforts in that an alternate collector structure is chosen, and the manufacturing process is geared more towards low-cost prototype development, than high-accuracy.

Point focus collectors experience optical inefficiencies when the reflective surface deviates from the ideal paraboloidal geometry. To attain high temperatures and power densities, surface contour errors of solar concentrators need to be minimised. Previously demonstrated manufacturing methods include diamond turning of aluminium to machine parabolic dishes to a root mean square (rms) mirror slope error of 0.1 mrad[6,7]. This process is expensive because of the materials and equipment involved, and suggests a need for novel, lower-cost manufacturing methods using composites. Such an approach has been followed here in the development of the ring array concentrator. To determine the feasibility of the manufacturing process, experimental characterisation of the high-flux solar energy is required.

Several devices have been developed for high-flux solar measurements, including calorimetric and the more expensive approach of radiometric techniques[8,9]. Calorimeters use energy balance methods to obtain estimated flux concentrations incident on the receiving surface. The methodology includes determining the heat absorbed by a heat transfer fluid flowing through the calorimeter body, by measuring the change in temperatures at inlet and outlet[10]. Considerations for this technique include minimising uncertain measurements pertaining to mass flow rate of the fluid and rise in temperature at calorimeter exit. Estimated modeling of heat losses due to convection and radiation is needed when the receiver plate does not approximate ambient temperature. Other more expensive instruments used for measuring heat-flux are concentrating photovoltaic (CPV) cells[11] and radiometers, such as the Gardon gauge[12]. For this study a low-cost approach was adopted to determine the performance of FOCUS using a flat plate calorimeter.

In this study we demonstrate the use of a ring array concentrator and fibre optic bundle to collect and transport solar energy for high energy flux applications. The optical fibres provide a means of transferring energy to a remote target, and controlling its delivery. As part of the study, ray tracing simulations are used to develop a predictive model of concentrator performance in the presence of optical errors. Thermal performance is characterised using energy balance theory with a flat plate calorimeter to validate the numerical model. Possible terrestrial and space-based research applications include solar power generation, CPV and lunar in-situ resource utilisation (ISRU).

2. FOCUS Solar Concentrating System

FOCUS consists of: a ring array concentrator, a fibre optic transmission line and a solar tracking system (figure 2). The prototype system is intended to supply thermal power to a variety of high temperature research projects, including a space related application in which lunar ISRU is exploited to reduce the cost of future moon missions. In the ISRU application, a minimum energy flux at fibre optic outlet of 85 W/cm^2 is required to demonstrate the successful melting of a commonly used regolith simulant called JSC–1A[13].

2.1 Ring array concentrator

The 600 mm diameter concentrator consists of seven mirror-like elements reflecting incoming direct normal irradiance into a fibre optic cable. Each reflective element can be adjusted horizontally in two dimensions to allow fine tuning of the focal spot. The collective reflective aperture area of the concentrator is 0.192 m^2.

2.2 Fibre optic transmission line

The fibre optic cable is manufactured by CeramOptec with a 0.37 numerical aperture consisting of 900 silica fibres treated to resist UV degradation. The bundle is 4 meters in length with estimated 95 % internal transmission efficiency and has fused 6 mm diameter inlet and outlet ends.

2.3 Solar tracking system

The concentrator array is equipped with a commercially available dual-axis solar tracker from Small Power Systems Inc. The average tracking accuracy of the sun sensor is 0.05°.

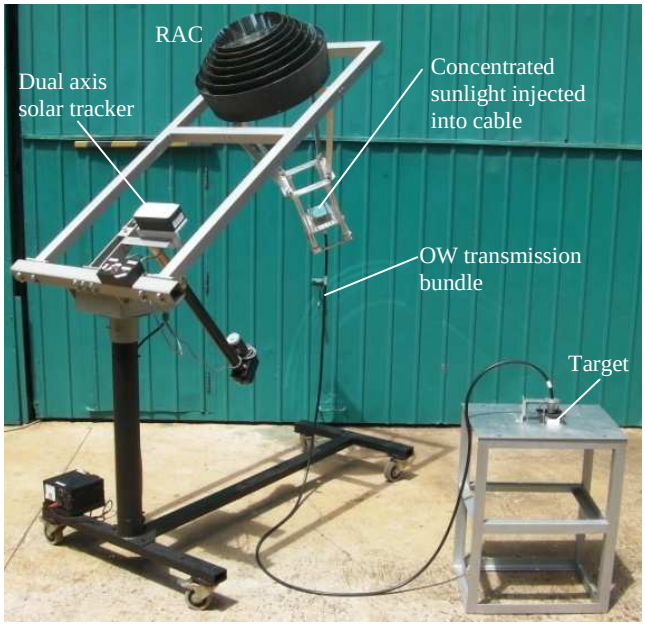

Figure 2: FOCUS ring array concentrator integrated with an optical waveguide bundle for high-flux level terrestrial and space applications

3. Collector Construction

The seven reflective elements of the ring array concentrator are manufactured using composite materials and a paraboloidal mould[14]. This approach is attractive because of the reductions in cost (one eighth the price of machining each ring from aluminium) and mass (3 kg reduction overall). Each reflective element is formed from a matrix material and two reinforcement materials to produce a fibre reinforced plastic composite. Starting with the largest diameter ring, the mould is machined using a CNC lathe and the wet lay-up is completed for that element (figure 3). The subsequent rings are manufactured individually by machining down the mould. The reflective surfaces of the ring array are laser cut into seven conic profiles from 95 % reflective Miro 4 aluminium of 0.4 mm thickness. The aluminium is strapped on to the mould and bonded together at the join with a rectangular sheet of aluminium as the connector (figure 4). The mould is vacuum bagged to allow the aluminium to form the shape of the paraboloid. After curing, silicone is beaded around the inner and outer diameters of the element to prevent resin seeping between the mould and profile surface. Glass and carbon fibre profiles are hand impregnated with resin and applied over the aluminium profile after which a second vacuum bagging process is conducted for additional consolidation of the geometry (figure 5). Glass and carbon fibre profiles were hand impregnated with resin for the wet lay-up and second vacuum bagging process. The concentration of sunlight with a completed reflective element is illustrated in figure 6.

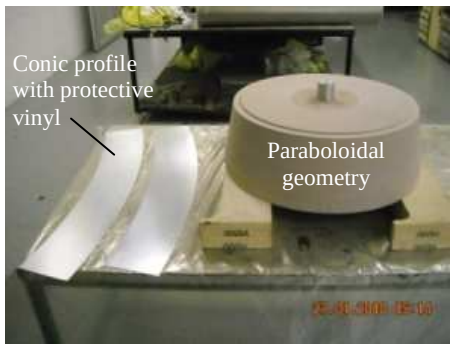

Figure 3: Machined geometry for element #1 (largest element) with conic aluminium profiles

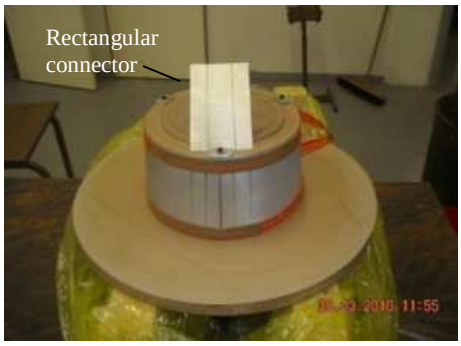

Figure 4: Profile for element #7 strapped to the tooling board mould before vacuum bagging process



Figure 5: Aluminium profile bonded with a bead of silicone to prevent resin offset between the metal surface and mould.

 © SAIMechE All rights reserved.



Figure 6: A completed reflective element focusing incident rays to a point.

Each element was optically analysed after fabrication to quantify surface errors resulting from the composite material manufacturing method.

In order to characterise optical errors for each reflective ring using slope measurements, the angular deviations between ideal and real perpendicular lines at specific points on each curved surface were obtained[15]. A three-dimensional co-ordinate measuring machine (CMM) was used to obtain slope errors[16,17], which lay between 5.67 mrad and 2.90 mrad rms (table 1). These are comparable to errors reported by Arasu and Sornakumar[18] and Johnston[19] who used similar fabrication methods for a parabolic trough and dish respectively. The general trend in the errors shows an increase in accuracy with decreasing diameter, highlighting the difficulty of manufacturing large, double-curvature, precision optics using composite materials.

Element	#1	#2	#3	#4	#5	#6	#7
RMSE (mrad)	4.77	5.67	5.39	4.02	3.32	4.22	2.90

Table 1: Root mean square error (RMSE) results for optically characterising the reflective elements

Several factors can cause surface errors in the manufactured elements, as well as variation in error between individual elements manufactured using the same method. For one, the manual wet lay-up, vacuum bagging process permits variation in the nature and extent of distortion. Variations in resin and fibre volume fractions also depend on the skill and consistency of the laminators. In this case, the nature of the wet lay-up process makes it difficult to produce consistent high fibre volume fractions for each of the seven elements. Improved slope error results in the smaller ring elements are due to the reduced curvature, with smaller elements requiring less shaping and pressure forming of the flat reflective aluminium to form a paraboloid. In addition the characteristic double curvature of the paraboloidal surface creates a complex manufacturing geometry in which material fibres are less likely to adhere accurately to the mould shape. The slope error results suggest that ring array designs should ideally comprise reflective elements with reduced curvatures if wet lay-up, vacuum bagging methods are employed. Despite the challenges of using composites in this type of application, we are able to demonstrate that low-cost reflective elements can be fabricated to reasonable accuracies, and for substantially reduced cost and weight.

4. Numerical Analysis

A numerical analysis was conducted using optical ray tracing software (OptisWorks Studio) to predict performance of the composite material concentrator. The optical efficiency of FOCUS (equation 1) can be estimated using results from the ray tracing exercise and is defined as the product of the efficiencies applicable to the concentrator (η_{RAC}), the focusing process (η_{foc}), injection into the fibre optic waveguide (η_{inj}) and transmission to the target (η_{τ}) (figure 7). Power values used to obtain the first three efficiency stages include the power at concentrator inlet (P_{in}), concentrator exit (P_{out}), inlet to optical waveguide (P_{OWin}) and the actual power injected into the silica fibres (P_{act}). Predictions of each power value were derived from the ray trace model.

$$\eta_{overall} = \eta_{RAC} \cdot \eta_{foc} \cdot \eta_{inj} \cdot \eta_{\tau} \qquad (1)$$

The power values given in figure 7 are based on a nominal input flux of 850 W/m^2 acting on an aperture of 0.192 m^2.

4.1 Ray tracing model

A ray tracing model was developed to characterise the optical efficiency of FOCUS by estimating the energy striking a receiver of 6 mm diameter, representative of the optical waveguide inlet. A further analysis was conducted to predict flux on a 60 mm diameter plate at the focal point of the collector, representative of the calorimeter used in experimental testing. Ray tracing simulations were conducted for eight cases describing the progression from ideal to realistic parameters. All eight cases employed a nominal direct normal irradiance of 850 W/m^2 to obtain comparative power density results. Table 2 shows the input parameters for each case. Representations of the best and worst case manufactured geometries were obtained from the CMM.

4.2 Ray tracing results

Figure 8 illustrates three dimensional flux maps at cable inlet for the ideal, unrealistic simulation of case 1 and the realistic worst case scenario of case 8. The no-loss model of case 1 shows flux magnitudes exceeding 46 000 suns that violate the second law of thermodynamics due to the omission of the solar half-angle in the ideal simulation. Implementing the

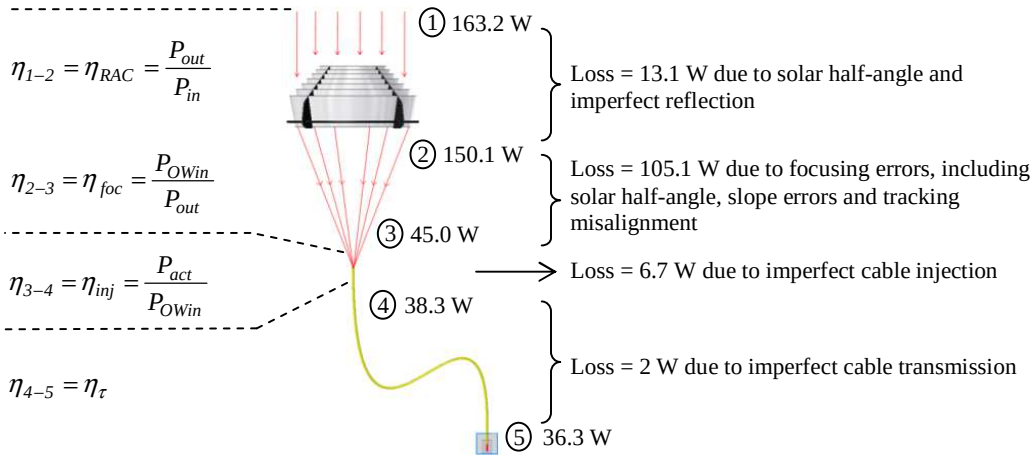

Figure 7: Predicted optical efficiency stages for FOCUS. The four efficiency stages include the concentrator, focusing process, injection into the optical waveguide and the transmission of the concentrated sunlight to the target

	Ideal							**Real**
Input parameters	**Case 1**	**Case 2**	**Case 3**	**Case 4**	**Case 5**	**Case 6**	**Case 7**	**Case 8**
Ideal parallel rays (0.00°)	1	0	0	0	0	0	0	0
Ideal specular reflection (100%)	1	1	0	0	0	0	0	0
Ideal RAC geometry	1	1	1	1	0	0	0	0
Ideal tracking error (0.00°)	1	1	1	0	1	0	1	0
Solar half-angle (0.265°)	0	1	1	1	1	1	1	1
Realistic specular reflection of mirror (95%)	0	0	1	1	1	1	1	1
Average tracking error (0.05°)	0	0	0	1	0	1	0	1
Manufactured geometry (Best case)	0	0	0	0	1	1	0	0
Manufactured geometry (Worst case)	0	0	0	0	0	0	1	1

Table 2: Ray tracing input parameters for 8 sets of numerical simulations conducted incorporating ideal and realistic parameters for comparison

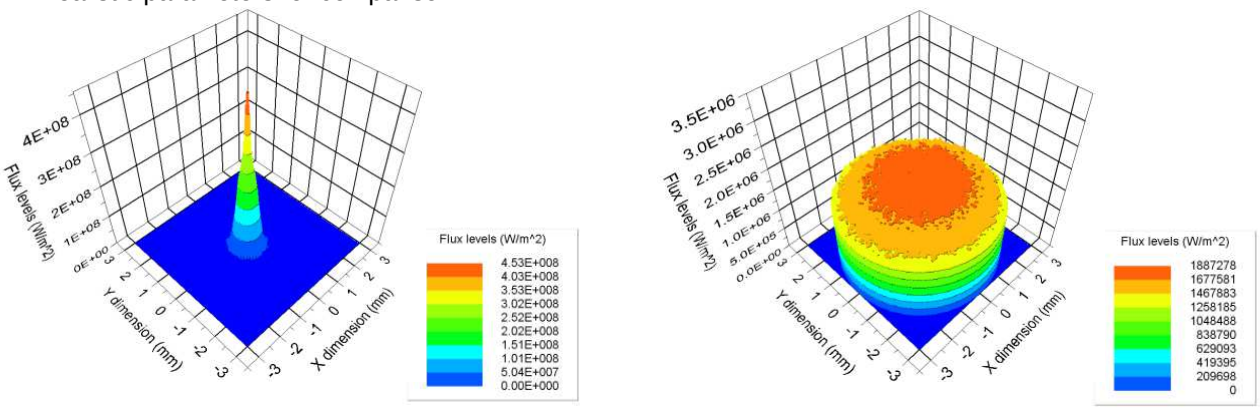

case 1 case 8

Figure 8: Three-dimensional flux maps representing flux levels at waveguide inlet for simulation cases 1 and 8

solar half-angle and other realistic parameters results in more uniform flux distribution within the 6 mm diameter area, as shown in the case 8 simulation. Figure 9 shows the cross-sectional flux profiles striking the 6 mm diameter inlet to the optical waveguide, F_{OWin}. Cases 2 – 8 describe, in a progressive manner, the expected losses at the fibre optic cable as successive error parameters are included. Optical waveguide inlet power decreases by 6% between cases 2 and 4, suggesting that tracking error and imperfect specular reflectance are relatively benign effects. A comparison between cases 4 and 6, and cases 4 and 8 illustrates slope error effects on the manufactured RAC.

For the manufactured best and worst case scenarios of the slope errors, a decrease in power of 45 % and 48 % is observed respectively. The primary aim of the numerical analysis is to predict flux profiles striking the 6 mm diameter fibre optic cable inlet using a worst case scenario. In addition a 60 mm diameter receiver was modelled to represent the flux profile striking the copper plate of the calorimeter, which is used in the experimental test procedure. Figure 10 illustrates the worst case flux profiles of case 8 for the 60 mm diameter and 6 mm diameter receivers. These are used to validate the experimental results against the numerical model.

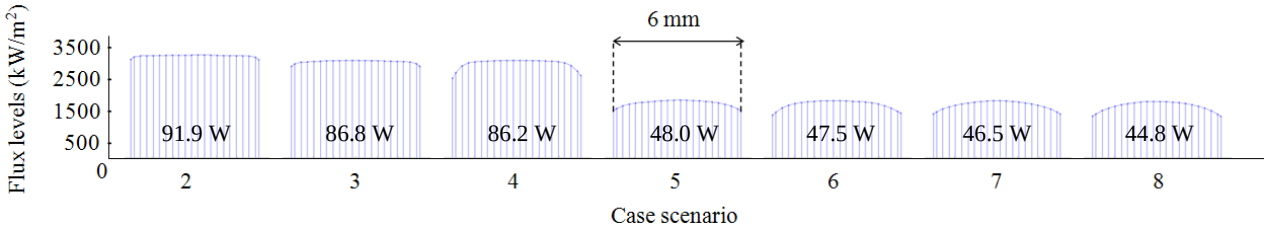

Figure 9: Two-dimensional flux maps showing modelled cross-sectional flux profiles at the 6 mm diameter optical waveguide inlet for Cases 2 - 8. Average power results striking the cable are given.

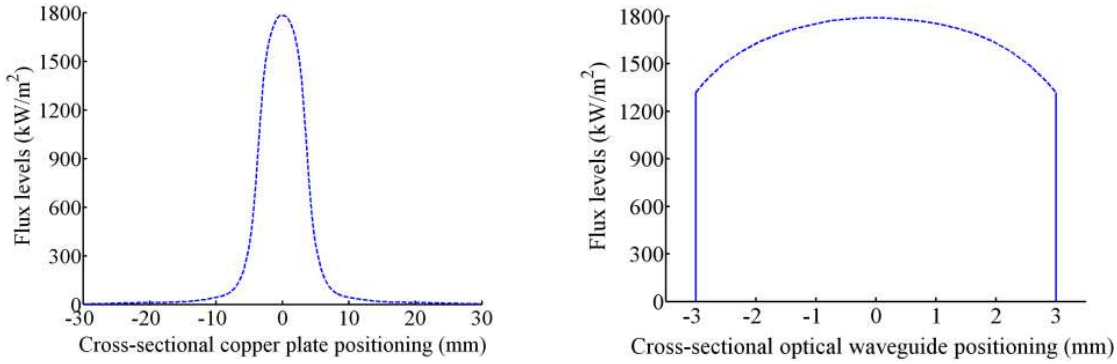

Figure 10: Representative cross-sectional flux maps showing the worst case ray trace scenario of case 8 for a 60 mm diameter copper receiver (left) and the fibre optic cable inlet (right).

The power values in figure 9 do not account for integration of the RAC with the fibre optic cable, therefore further processing of the ray trace results is needed to estimate the energy injected into and transmitted through the cable. Using case 8 as an example, the inlet power of 44.8 W to the cable is scaled down by factoring the collective area of the fibres and the expected transmission efficiency of the cable, as described in the design methodology[13]. Table 3 summarises the expected power, P, flux, F, and flux concentration, C_{flux}, entering (OW_{in}) and exiting (OW_{out}) the cable and overall optical efficiency results of FOCUS.

		Case 1	Case 2	Case 3	Case 4	Case 5	Case 6	Case 7	Case 8
Stages	η_{RAC}	1.00	0.98	0.93	0.93	0.93	0.93	0.92	0.92
	η_{foc}	1.00	0.58	0.58	0.57	0.32	0.31	0.31	0.30
	η_{inj}	0.85	0.85	0.85	0.85	0.85	0.85	0.85	0.85
	η_{τ}	0.95	0.95	0.95	0.95	0.95	0.95	0.95	0.95
Total	$\eta_{overall}$	0.81	0.46	0.44	0.43	0.24	0.23	0.23	0.22
Power at cable inlet, P_{OWin} (W)		163.2	91.9	86.8	86.2	48.0	47.5	46.5	44.8
Fibre optic inlet flux, F_{OWin} (W/cm^2)		577.2	325.0	307.0	304.9	169.8	168.0	164.5	158.4
Flux concentration, cable inlet, $C_{flux,\ OWin}$ (suns)		6790.6	3823.9	3611.7	3586.7	1997.2	1976.4	1934.8	1864.1
Power at cable outlet, P_{OWout} (W)		132.4	74.5	70.4	69.9	38.9	38.5	37.7	36.3
Fibre optic outlet flux, F_{OWout} (W/cm^2)		548.3	308.8	291.6	289.6	161.3	159.6	156.2	150.5
Flux concentration, cable outlet, $C_{flux,\ OWout}$ (suns)		6451.1	3632.7	3431.1	3407.4	1897.4	1877.6	1838.1	1770.9

Table 3: Predicted component efficiencies and average performance results for FOCUS using ray tracing methods at a typical irradiance of 850 W/m^2

5. Experimental Results

The experimental testing programme aimed to characterise performance of FOCUS using energy balance methods in conjunction with a flat plate calorimeter. Testing was conducted in three phases to determine firstly the power entering and secondly exiting the fibre optic cable and thirdly the melting capabilities of a lunar regolith stimulant using FOCUS.

5.1 Energy balance methodology

The flat plate calorimeter consists of a stainless steel outer casing, a nylon insulator and a copper receiving plate (figure 11). An energy balance was carried out on the calorimeter to determine the concentrated flux arriving at the plate surface. A detailed heat transfer analysis using the flat plate calorimeter is described by Mouzouris *et al.*[20]. During operation, concentrated rays strike the copper disc while cold water flows through the device to absorb energy. The energy balance is invoked to estimate the solar power incident on the plate, q_{in}, by summing the energy absorbed by the water flow, q_{abs}, and the external heat losses due to radiation and convection, $q_{l,out}$ (equation 2). External heat losses are estimated using temperature measurements midway in the copper plate. The absorptivity of the plate surface, α_s, estimates the fraction of incident irradiation absorbed. Internal losses are neglected due to the low thermal conductivity of the nylon insulation within the calorimeter body.

$$\alpha_s q_{in} = q_{abs} + q_{l,out} \qquad (2)$$

5.2 Experimental setup

Key components of the experiment include FOCUS, the calorimeter, water circulation system and instrumentation (figure 12). To determine the high-flux solar measurements of FOCUS, the calorimeter is positioned first at the focal point of the concentrator, and secondly at fibre optic cable exit. Positioning the calorimeter at concentrator focus allows the parameter at optical waveguide inlet to be determined such as power, (P_{OWin}) flux (F_{OWin}) and flux concentration ratio ($C_{flux,OWin}$). When the calorimeter is placed at fibre optic outlet, P_{OWout}, F_{OWout} and $C_{flux,OWout}$ are characterised.

5.3 Experimental procedure

Experimental testing was conducted at the University of KwaZulu-Natal under clear sky conditions. The test area is sheltered from wind while allowing clear vertical views for sun-concentrator orientation. Direct normal irradiance (DNI) was measured with an Eppley Normal Incidence Pyrheliometer at the nearby Howard College radiometric ground station (29.9°S, 30.98°E at 151.1 m elevation[21]). A typical experiment includes cleaning the seven reflective elements and positioning them such that the focal spot approximates concentric alignment onto the receiver, being either the copper plate or the fibre optic cable inlet. The receiver is firstly positioned using the calculated focal point and then fine-tuned to minimise the focal spot diameter. Positioning the ring elements and receiver was performed with the dual-axis solar tracker in operation. Running time per experiment was three minutes. The fluid circulation system consists of a pump fitted with a throttle valve to achieve the desired mass flow rate. Mass flow

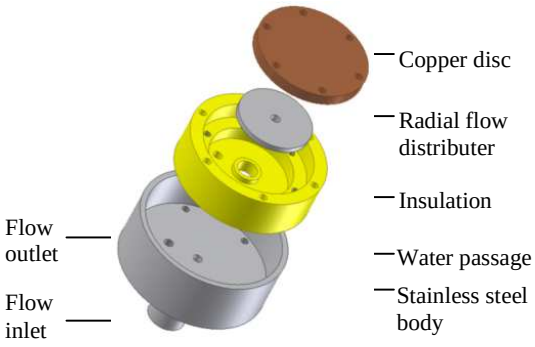

Figure 11a: Exploded view of the flat plate calorimeter constructed for performance measurements of FOCUS

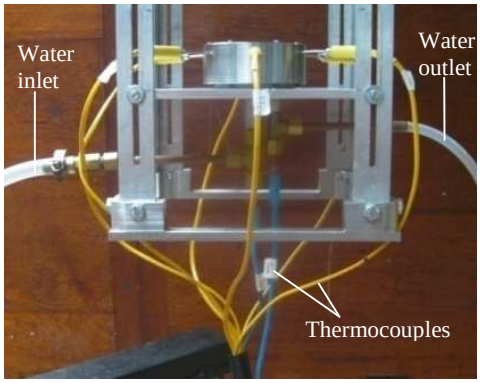

Figure 11b: Calorimeter side view showing water inlet and and outlet passages

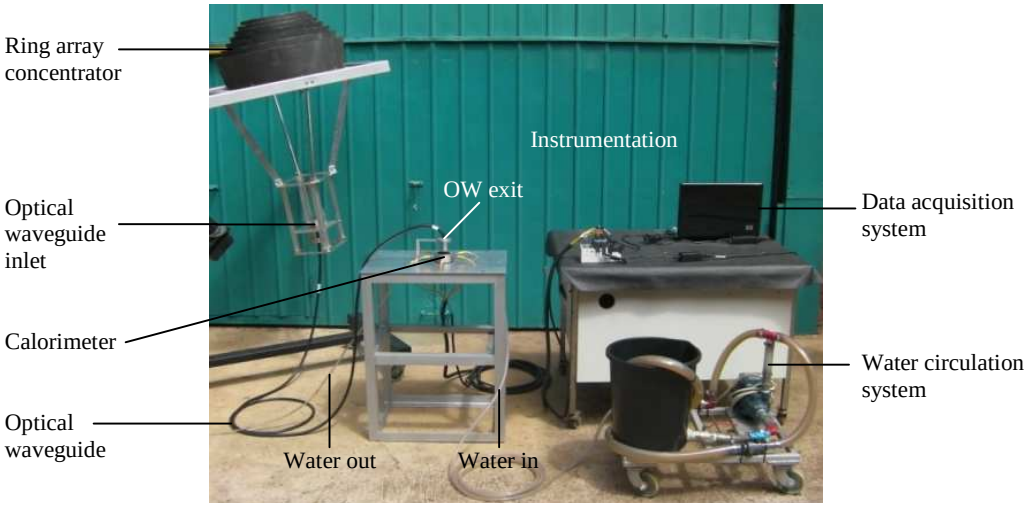

Figure 12: Experimental layout to characterise the energy flux at the optical waveguide exit, including key components FOCUS, the flat plate calorimeter, water circulation system and thermocouples.

rate, $\dot{m}$, is measured by conducting a timed volume collection and is set to keep the copper receiving plate at a temperature close to ambient to minimise external heat losses due to convection and radiation. Instrumentation includes two type T thermocouples for the inlet, T_{in}, and outlet, T_{out}, water measurements and six type K thermocouples for the temperature distribution measurements midway in the copper plate. The six thermocouples are labelled T_0, T_5, T_{10}, T_{15}, T_{20} and T_{25} and are used to estimate the surface temperature, T_s of the copper plate.

5.3.1 Concentrator focus results

Characterising the flux distribution at concentrator focus requires covering the copper plate of the calorimeter with a series of reflective shields to progressively limit exposure of concentrated rays onto the copper receiver. Ten stages were chosen for discretising the flux distribution, starting with no shield, representing full exposure of the copper plate, and ending with a reflective shield incorporating a 3 mm diameter opening. The 6 mm diameter reflective shield represents the cable inlet (figure 13). A nylon backing is applied to minimise conduction between the shield and copper surface. Several experiments were

conducted for each shield to obtain the average power incident on the exposed copper surface. Subtracting successive exposed power values yielded a discretised flux distribution pattern for the 60 mm diameter receiver.

Data from a typical experiment using the 6 mm diameter reflective shield are shown in table 4. The calorimeter inlet and outlet water temperatures and temperature distributions midway in the copper plate are shown in figure 14. Of importance is the stabilisation of temperature measurements which allows for the assumption of steady state conditions. A temperature difference between water inlet and outlet of 6.4 °C is observed after three minutes allowed for stabilisation, using a mass flow rate of 0.00154 kg/sec resulting in 41 W of power absorbed by the water. To obtain an estimate power striking the copper plate surface, heat losses were calculated using the temperature distribution midway in the copper plate and added to the power absorbed by the water. The temperature measurements of T_{10}, T_{15} and T_{20} show unexpected similar readings with possible reasons due to thermocouple inaccuracies or imprecise machining of the copper plate. Heat losses due to convection and radiation amounted to 0.2 % of the power absorbed, resulting in an estimate power striking the copper plate surface of 43.2 W at an irradiance of 938.0 W/m^2. This corresponds to an efficiency of 24 % which is in good agreement with the case 8 numerical efficiency result at optical waveguide inlet of 27 %.

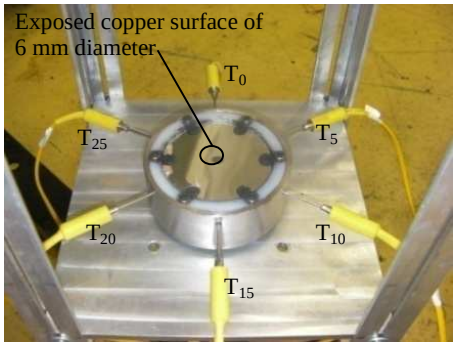

Figure 13: The 6 mm diameter reflective shield positioned at concentrator focus

A comparison between experimental and modelled flux for the parameter set of Case 8 is shown in Figure 15. Experimental results show a peak flux level of 1528 kW/m^2 at an input irradiance of 850 W/m^2, corresponding to a concentration of 1798 suns. Measured maximum temperature values at concentrator focus approached 1500°C at irradiance levels in the region of 1000 W/m^2. Measured flux obtained from the application of successive discretised filters, closely follows predicted flux from the ray tracing exercise. Experiments conducted using smaller reflective shields allowing a 2 mm and 1 mm diameter exposure of the copper surface produced inconsistent results, possibly due to measurement uncertainties at very low heat transfer rates.

	Experiment
Average irradiance level (W/m^2)	938.0
Ray trace q_{in} (W)	48.8
Experimental q_{in} (W)	43.2
q_{abs} (W)	41.0
$q_{l,out}$ (W)	0.09
$\dot{m}$ (kg/s)	0.00154
ΔT (T_{out} - T_{in}) (°C)	6.4
T_s (°C)	69.2
T_{in} (°C)	27.0
T_{out} (°C)	33.4
Experimental q_{in} normalised to 850 W/m^2 (W)	39.2

Table 4: Experimental measurements and results for a typical experiment using a reflective shield with 6 mm aperture.

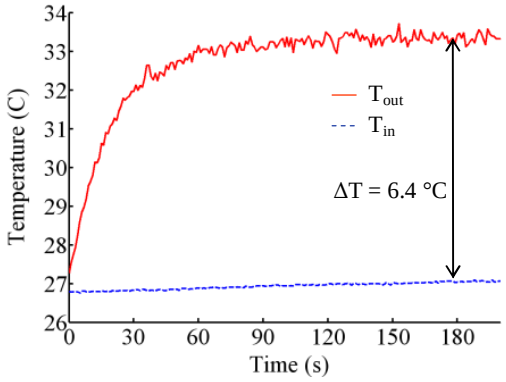

Figure 14a: Results from a typical experiment, showing a water temperature difference of 6.4 °C

Difficulties in stabilising the system for very small diameter filter plates (< 3 mm) resulted in poor resolution near the peaks of both curves in figure 15. This is a shortcoming in the calorimetric method of measuring flux. To measure peak flux levels, further performance testing using a radiometric device such as a Gardon flux sensor is indicated.

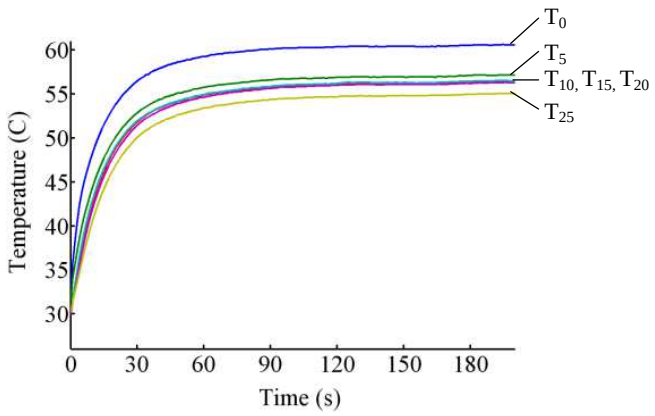

Figure 14b: Results from a typical experiment, showing temperature measurements midway in the copper plate

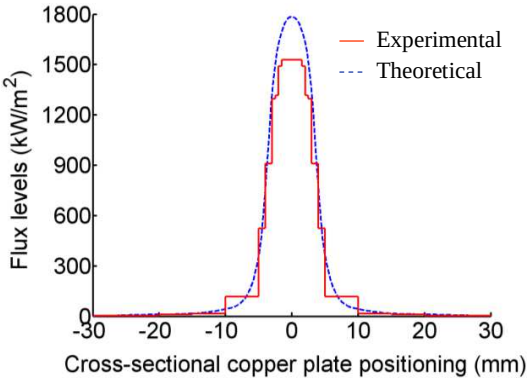

Figure 15a: Performance results at concentrator focus showing flux levels striking the 60 mm diameter copper plate (at 850 W/m^2)

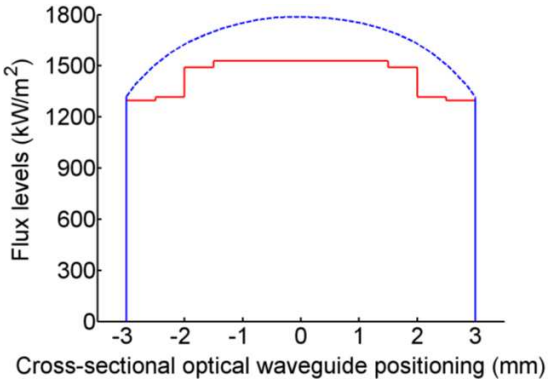

Figure 15b: A magnified view of the 6 mm diameter inlet to the optical waveguide (at 850 W/m^2)

Key results from the first phase experiments include performance at optical waveguide inlet. Representative average power and flux levels incident on the cable of 39.4 W and 139.3 W/cm^2 respectively were observed over five experiments. An injected power into the 900 silica fibres of 33.5 W is estimated and is used in calculating the transmission efficiency of the cable.

5.3.2 Optical waveguide exit results

Waveguide exit performance results are obtained by directing the cable outlet at the calorimeter, as shown in figure 16a. Tests were conducted using the same methodology as at concentrator focus, but without the reflective shields. A shield was positioned at optical waveguide inlet to protect the metal ferrule from stray radiation that may cause damage (figure 16b). The shield restricts energy to the 6 mm diameter quartz glass inlet of the cable. At cable outlet a preventative measure of offsetting the cable 5 mm away from the calorimeter centre, was taken to avoid reflection of sunlight back on to the fibre bundle.

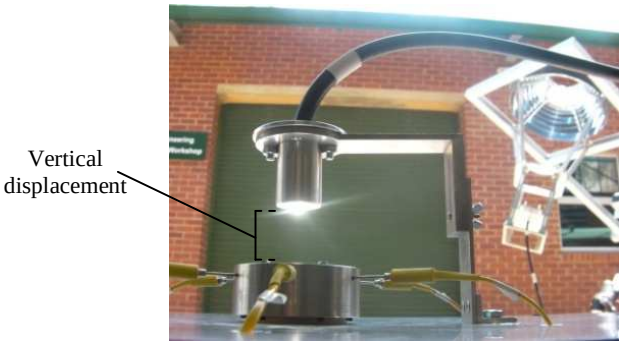

Figure 16a: Vertical displacement of the cable outlet prevents damaging back reflection on to the 900 fibres of the cable

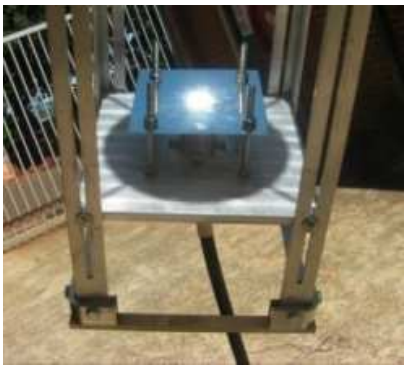

Figure 16b: Reflective shield at fibre optic cable inlet allowing concentrated solar energy into the 6 mm diameter quartz glass inlet

 © SAIMechE All rights reserved.

Test results showed an average power of 20.5 W exiting the cable and striking the copper plate at a vertical displacement of 5 mm, corresponding to a flux of 84.9 W/cm^2 in the exit plane of the fibres. The results represent normalised values at a direct normal irradiance of 850 W/m^2. Transmission efficiency of the fibre optic cable is estimated at 61 % using the average power results from the 6 mm diameter reflective shield, conducted at concentrator focus. A predicted efficiency of 95 % was used for the theoretical calculations stipulated by the supplier of the cable. A possible reason for the 34 % decrease in efficiency is greater losses due to reflection at inlet to the cable. The reflective losses at cable inlet result from the sudden change of refractive index from air (n = 1.0) to fused quartz glass (n = 1.5). This was not modelled in the ray tracing simulation. A possible solution to minimise inlet reflective losses is the design and implementation of a secondary concentrator at cable inlet to boost energy injection into the silica fibres.

5.3.3 Optical efficiency

Final performance results from the first two experimental phases are given in table 5. A predicted efficiency of 22 % was obtained using ray tracing methods and a worst case error set. Experimental results show an efficiency of 13 %, with the difference attributed mainly to high reflective losses at inlet to the optical fibres.

	Theoretical	Experimental
P_{OWin} (W)	44.8	39.4
F_{OWin} (W/cm^2)	158.4	139.3
$C_{flux,\ OWin}$ (suns)	1864.1	1638.8
P_{OWout} (W)	36.3	20.5
F_{OWout} (W/cm^2)	150.5	84.9
$C_{flux,\ OWout}$ (suns)	1770.9	998.8
$\eta_{overall}$	0.22	0.13

Table 5: FOCUS experimental performance (data normalised to a direct normal irradiance of 850 W/m^2 - average of five tests)

5.3.4 Regolith melting capabilities

In the final test procedure, several melting experiments were performed in which concentrated sunlight was directed at a sample of the lunar regolith simulant, JSC-1. This was intended to demonstrate the high surface temperatures and flux levels required to melt lunar regolith for ISRU-related applications, such as those reported by Nakamura and Senior[7]. The experimental procedure includes positioning the optical waveguide onto the JSC-1 surface and measuring the the temperature of the melt zone formed after a period of six minutes (figure 17a). A downward facing reflective shield was positioned beneath the cable to prevent reflected solar rays from the regolith surface striking the cable. The temperature of the regolith simulant was measured using a thermocouple positioned at the centre of the melt zone. Figure 17b shows a post-experimental sample of the melted regolith from a typical experiment. The vitrified circular melt zone formed after six minutes is 6 mm in diameter, with a depth of 2.5 mm.

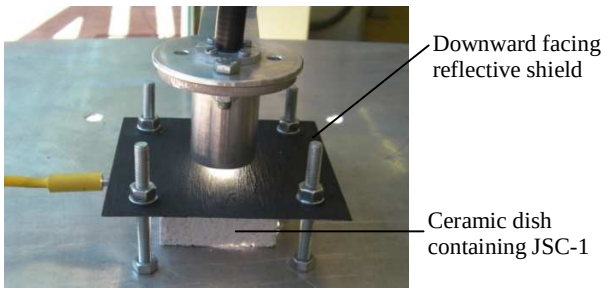

Figure 17a: Regolith melting experiment with the protective shield (reflector) to prevent cable damage and a thermocouple

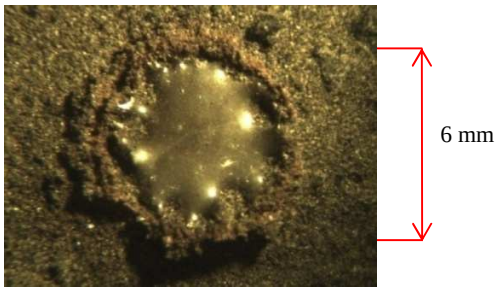

Figure 17b: Magnified view of the vitrified melt with diameter of 6 mm and depth 2.5 mm

Table 6 summarises the peak melt temperature readings obtained for five separate experiments. The stabilisation of temperature within the melt zone is illustrated in figure 18, showing peak values graphed against estimated flux levels. Flux levels exiting the cable were estimated using average irradiance levels over the test period and the optical efficiency value of 13 %. Results show a peak temperature exceeding 1200 K at cable exit flux levels of 104 W/cm^2 which exceeds the minimum flux criterion for successful regolith melting by 22 %. Temperature results achieved can be applied to several high temperature lunar ISRU processes, including oxygen production and surface stabilisation. Creating larger sintered surfaces for practical human use on the lunar surface is possible by implementing autonomous mechanisms to drive multiple fibre optic cables in a coordinated manner[22].

	Experiment				
	#1	**#2**	**#3**	**#4**	**#5**
Irradiance level (W/m^2)	1005.4	997.1	995.7	991.3	987.9
Peak temperature (°C)	935.5	901.6	882.0	876.9	850.4
Flux level (W/cm^2)	104.0	103.1	102.9	102.5	102.1

Table 6: Lunar regolith simulant peak melt temperature and cable exit flux concentration results

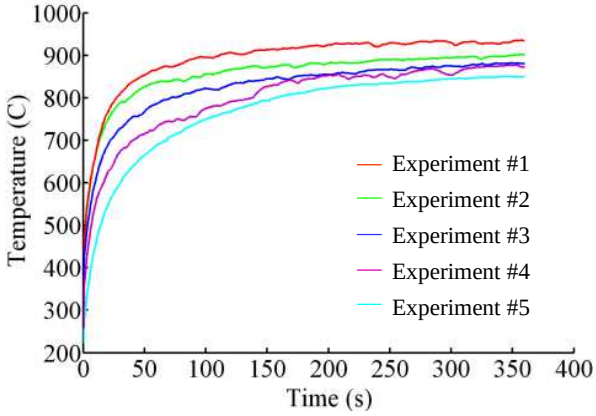

Figure 18a: Time evolution of the melt temperature for five experiments for 6 min showing temperature stabilisation in the melt zone

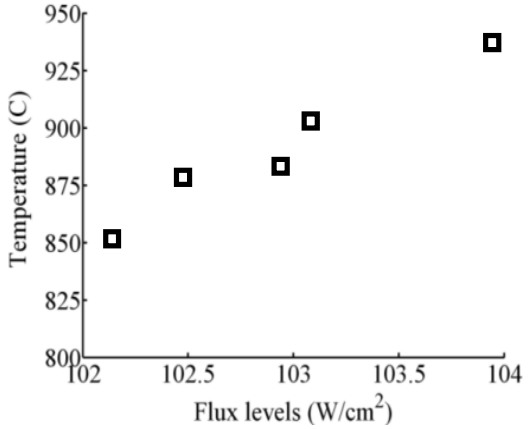

Figure 18b: Peak melt temperatures versus maximum flux levels exiting the 900 silica fibres

6. Conclusion

The design, fabrication and testing of a composite material ring array concentrator is described for the collection of solar energy and its transmission through a fibre optic bundle. The FOCUS system has application in high-temperature research such as material sintering and lunar in-situ resource utilisation. The overall transmission efficiency from aperture to bundle outlet was measured at 13 % using a flat plate calorimeter. Temperatures exceeding 1450 °C and 900 °C were measured at the concentrator focal point and the outlet of the fibres respectively, yielding flux levels of 104 W/cm^2. An optical error analysis of the seven reflective elements is described. In addition to performance validation, this work also provides an alternate approach to conventional methods of collector construction. Rather than machining metal profiles for the reflective surface, extensive use was made of composite materials, resulting in a low-cost, light weight point focus concentrator that is 38 % lighter than an aluminium equivalent and considerably less expensive. Results suggest that further reduction in optical error is possible by limiting reflector curvature in the design stage and adapting the optics to accommodate for structural distortion during curing.

Acknowledgements

The authors appreciate the assistance and support of Professor J. Bindon, Professor W.H. Moolman, Clinton Bemont, Khulisile Kunene, Michael Constantino, OPTIS, Durban University of Technology and the University of Stellenbosch's Centre for Renewable and Sustainable Energy Studies (CRSES). This work is supported by the National Research Foundation of South Africa and the Eskom TESP program.

References

1. *Pregger T, Graf D, Krewitt W, Sattler C, Roeb M and Moller S,* Prospects of solar thermal hydrogen production processes, *International Journal of Hydrogen Energy*, 2009, 34, 4256-4267.
2. *Kalogirou SA,* Solar thermal collectors and applications, *Progress in Energy and Combustion Science*, 2004, 30, 231-295.
3. *Sen Z,* Solar energy in progress and future research trends, *Progress in Energy and Combustion Science*, 2004, 30, 367-416.
4. *Vasylyev S and Vasylyev V,* Nonimaging reflective lenses: A new type of high-heat solar collector, *Proceedings of the Solar World Congress*, Orlando, Florida, 2005.

 © SAIMechE All rights reserved.

5. *Vasylyev V and Vasylyev S,* Expected optical performances of novel type multi-element high-heat solar concentrators, *Proceedings of the American Solar Energy Society,* Reno, NV, 2002.
6. *Feuermann D, Gordon JM and Huleihil M,* Solar fiber-optic mini-dish concentrators: First experimental results and field experience, *Solar Energy,* 2002, 71, 459-472.
7. *Nakamura T and Senior CL,* Solar thermal power for lunar materials processing, *Journal of Aerospace Engineering,* 2008, 21, 91-101.
8. *Ballestrín J, Estrada CA, Rodríguez-Alonso M, Pérez-Rábago C, Langley LW and Barnes A,* Heat flux sensors: Calorimeters or radiometers? *Solar Energy,* 2006, 80, 1314-1320.
9. *Ballestrín J,* A non-water-cooled heat flux measurement system under concentrated solar radiation conditions, *Solar Energy,* 2002, 73, 159-168.
10. *Estrada CA, Jaramillo OA, Acosta R and Arancibia-Bulnes CA,* Heat transfer analysis in a calorimeter for concentrated solar radiation measurements, *Solar Energy,* 2007, 81, 1306-1313.
11. *Fernandez-Reche J, Sanchez M, Alonso M, Canadas I, Chenlo F, Rodriguez J and Ballestrin J,* Concentrating PV: An alternative to calorimeters for measuring high solar flux densities, *Journal of Solar Energy Engineering,* 2008, 130, 0445021-0445023.
12. *Ballestrín J, Ulmer S, Morales A, Barnes A, Langley LW and Rodriguez M,* Systematic error in the measurement of very high solar irradiance, *Solar Energy Materials and Solar Cells,* 2003, 80, 375-381.
13. *Mouzouris M and Brooks MJ,* Nonimaging solar thermal collector for high temperature terrestrial and space applications, *Proceedings of SPIE Optics and Photonics,* San Diego, CA, 2009.
14. *Mouzouris M and Brooks MJ,* Construction of a composite material solar concentrator for high heat flux applications, *Proceedings of 8th Annual International Energy Conversion Engineering Conference,* Nashville, TN, 2010.
15. *Stine WB and Harrigan RW,* Solar energy fundamentals and design: with computer applications, *Wiley, Alternate Energy,* 1985, 185-188.
16. *Kumler JJ and Caldwell JB,* Measuring surface slope error on precision aspheres, *Proceedings of SPIE Optics and Photonics,* 2007.
17. *Menq C and Chen FL,* Curve and surface approximation from CMM measurement data, *Computers ind. Engng,* 1996, 30, 211-225.
18. *Arasu VA and Sornakumar T,* Design, manufacture and testing of fiberglass reinforced parabola trough for parabolic trough solar collector, *Solar Energy,* 2007, 81, 1273-1279.
19. *Johnston G,* Focal region measurements of the 20 m^2 tilted dish at the Australian National University, *Solar Energy,* 1998, 63, 117-124.
20. *Mouzouris M, Roberts LW and Brooks MJ,* Heat transfer analysis for high-flux solar measurements using a flat plate calorimeter, *Proceedings of First Postgraduate Renewable Energy Symposium CRSES,* Stellenbosch, RSA, 2010.
21. *Kunene KR, Brooks MJ, Roberts LW and Zawilska E,* Introducing GRADRAD: The greater Durban radiometric network, *Proceedings of World Renewable Energy Congress XI,* Abu Dhabi, UAE, 2010.
22. *Nakamura T and Smith BK,* Solar thermal system for lunar ISRU applications: Development and field operation at Mauna Kea, HI, *Proceedings of 48th AIAA Aerospace Sciences Meeting Including the New Horizons Forum and Aerospace Exposition,* Orlando, FL, 2011.

 © SAIMechE All rights reserved.